




Article

Net Forest Carbon Loss Induced by Forest Cover Change and Compound Drought and Heat Events in Two Regions of China

Chenfeng Gu ^{1,2} , Tongyu Wang ^{1,2}, Wenjuan Shen ^{1,2,*} , Zhiguo Tai ^{1,2}, Xiaokun Su ^{1,2}, Jiaying He ³, Tao He ⁴ , Weishu Gong ⁵ and Chengquan Huang ⁵

¹ Co-Innovation Center for Sustainable Forestry in Southern China, Nanjing Forestry University, Nanjing 210037, China; guchenfeng@njfu.edu.cn (C.G.); ty_w@njfu.edu.cn (T.W.); taizhiguo@njfu.edu.cn (Z.T.); suxiaokun1201@njfu.edu.cn (X.S.)

² Department of Forest Resources Management, College of Forestry and Grassland, Nanjing Forestry University, Nanjing 210037, China

³ State Key Laboratory of Resources and Environmental Information System, Institute of Geographic Sciences and Natural Resources Research, Chinese Academy of Sciences, Beijing 100101, China; hejiaying@igsrr.ac.cn

⁴ School of Remote Sensing and Information Engineering, Wuhan University, Wuhan 430079, China; taohers@whu.edu.cn

⁵ Department of Geographical Sciences, University of Maryland, College Park, MD 20742, USA; wsgong@umd.edu (W.G.); cqhuang@umd.edu (C.H.)

* Correspondence: wjshen@njfu.edu.cn

Abstract: Compound drought and heat events (CDHEs) and forest cover change influence regional forest carbon dynamics. Changes in regional vegetation biomass and soil carbon storage induced by forest cover change often exhibit considerable uncertainty, and previous research on the impacts of CDHEs on forest carbon dynamics is limited. To accurately quantify the specific effects of forest cover change and CDHEs on forest carbon dynamics in different regions, we employed a combined algorithm of the Carnegie–Ames–Stanford Approach (CASA) and bookkeeping empirical models to examine the impact of regional forest cover changes on forest carbon dynamics during 2000–2022 in Nanjing and Shaoguan, Southern China. Using the Geographical Detector model, we then analyzed the effects of CDHEs on forest carbon dynamics. Next, we used the photosynthesis equation and the optimal response time of forests to drought (heat) events to calculate the changes in forest carbon sequestration caused by CDHEs in both regions during 2000–2022. The results indicated that afforestation and deforestation led to +0.269 TgC and +1.509 TgC of carbon sequestration and 0.491 TgC and 2.802 TgC of carbon emissions in Nanjing and Shaoguan, respectively. The overall effects of CDHEs on the change in forest carbon sequestration were manifested as net carbon loss. In Nanjing, the net carbon loss caused by CDHEs (0.186 TgC) was lower than the loss due to forest cover change (0.222 TgC). In Shaoguan, the net forest carbon loss caused by CDHEs (3.219 TgC) was much more significant than that caused by forest cover change (1.293 TgC). This study demonstrated that forest carbon dynamics are dominated by different factors in different regions, which provides a scientific basis for local governments to formulate targeted forest management policies.

Keywords: compound drought and heat events; forest cover change; bookkeeping model; geographical detector; carbon storage



Citation: Gu, C.; Wang, T.; Shen, W.; Tai, Z.; Su, X.; He, J.; He, T.; Gong, W.; Huang, C. Net Forest Carbon Loss Induced by Forest Cover Change and Compound Drought and Heat Events in Two Regions of China. *Forests* **2024**, *15*, 2048. <https://doi.org/10.3390/f15112048>

Academic Editor: Radu-Daniel Pintilii

Received: 21 October 2024

Revised: 18 November 2024

Accepted: 18 November 2024

Published: 20 November 2024



Copyright: © 2024 by the authors. Licensee MDPI, Basel, Switzerland. This article is an open access article distributed under the terms and conditions of the Creative Commons Attribution (CC BY) license (<https://creativecommons.org/licenses/by/4.0/>).

1. Introduction

Extreme weather events and land cover change significantly impact global terrestrial ecosystem carbon cycling [1–4]. Drought and heat events, as typical extreme climate events, directly weaken vegetation photosynthesis through water and heat stress, potentially leading to vegetation mortality and reducing ecosystem carbon uptake, further releasing large amounts of forest carbon [5–7]. Land cover change leads to shifts in terrestrial carbon stocks [8]. Forest is the largest carbon reservoir of the terrestrial ecosystem, and

frequent afforestation and deforestation activities change the land cover and affect the carbon balance, which deserves attention [9,10]. Therefore, precisely quantifying the effects of forest cover change and compound drought and heat events (CDHEs) on forest carbon dynamics is vital for understanding how human activities and extreme climate events influence the forest carbon balance.

Over the past few decades, numerous studies have been undertaken to enhance our comprehension of the effects of CDHEs on forest carbon dynamics. For instance, Zhao et al. [11] found that during the 2022 CDHEs in the Yangtze River Basin, low soil moisture (SM) and a high vapor pressure deficit (VPD) were the primary factors contributing to reduced forest productivity. Li et al. [12] showed that high temperatures significantly impacted gross primary productivity (GPP) reduction, followed by low soil moisture. VPD contributed the least through multiple linear regression analysis of the impact of various indicators on GPP during July–October 2022. Nevertheless, most research investigating the effects of CDHEs on forest carbon dynamics relies on correlation, regression, and trend analysis methods. These studies presume notable linear relationships between related factors and vegetation growth [13–15]. Yet, the responses of terrestrial vegetation to various influences can be intricate, and relying solely on linear statistical methods may not suffice to portray these relationships accurately [13]. While copula-based models have been used to study the interaction of CDHEs and vegetation, they may not precisely distinguish the specific interactions of CDHEs [13–15]. Geographical Detector (GD) is a model for exploring spatial heterogeneity in vegetation and its relevant factors, pinpointing the importance and degree of diverse driving factors (meteorological, geographical, and human activities, etc.) and elucidating the interplay between these factors and vegetation [16,17]. However, these models have not gained widespread application in analyzing the effects of CDHEs on forest carbon dynamics. Simultaneously, few efforts have been made to quantify changes in regional forest carbon sequestration due to CDHEs.

In recent years, optical, radar, and LiDAR remote sensing observations have facilitated the understanding and monitoring of land cover changes and vegetation dynamics worldwide and on regional scales. They have refined carbon flux models and enhanced quantitative predictions of ecosystem carbon balance impacts [9,18]. In recent decades, numerous approaches and models have been utilized to assess forest carbon fluxes and reservoirs. Observing changes in atmospheric CO₂ concentrations can help to infer forest carbon sources and sinks [19], albeit with significant uncertainties. Inventory methods relying on forest survey data, such as Zeng et al. [20], used the National Forest Inventory (NFI) to assess changes in forest carbon stocks in China over 70 years (1948–2018). However, the uncertainty is significant on a regional scale. Process-based ecosystem models can simulate changes in forest carbon stocks but often operate at coarse spatial resolutions, leading to significant discrepancies between simulated and observed values [21,22]. For example, Zhao and Zhuang [23] utilized the Peatland version of the Terrestrial Ecosystem Model (PTEM) to estimate carbon dynamics in peatlands across northern high latitudes, encompassing the timeframe from 1990 to 2300. However, the model's spatial resolution of 0.5° is insufficient to capture the effects of regional-scale forest cover changes.

Bookkeeping models track carbon fluxes generated by land use change and forest disturbance and perform well in regional or global ecosystem assessments [24,25]. However, they lack spatially distributed carbon flux data and assume that carbon density remains constant over time, resulting in significant differences from observational data. Due to classification errors and other factors in regional land use/land cover change data, there is considerable uncertainty in estimating ecosystem carbon budgets at finer local and regional scales [26,27]. The CASA model is a light energy utilization model combined with the principle of photosynthesis, and its parameters are small and easy to obtain, making it easy to apply [28]. It can be combined with remote sensing data to obtain different spatial scale net primary productivity (NPP) data for small-scale regions. Therefore, we intend to incorporate the CASA model with the bookkeeping model to assess forest carbon dynamics due to forest cover change at the regional scale.

So far, numerous scholars have employed diverse methods and models, successfully quantifying the impacts of forest cover changes and CDHEs on the forest carbon cycle within the Yangtze River Basin and across China [29–31]. However, few studies accurately quantify regional forest cover change and its effects on forest dynamics with high spatial resolution. Both Nanjing and Shaoguan have subtropical monsoon climates (Table 1). However, the former belongs to the North subtropical zone, and the latter belongs to the Middle subtropical zone. The primary land use type in Shaoguan is forest, while it is farmland in Nanjing. Shaoguan, as a typical forest city in Guangdong Province, has a low level of urbanization and slow economic development. Nanjing is a major financial city in the Yangtze River Delta, with a high level of urbanization and a developed economy. Meanwhile, the forest coverage rate ranks first in Jiangsu Province, China. Since 2000, forest cover changes and CDHEs have occurred more frequently in these two regions. Therefore, quantitatively comparing and exploring the difference between forest cover change and CDHEs on forest carbon dynamics in these regions is of particular social, economic, and ecological value. Furthermore, it is crucial to contrast the disparities in forest carbon dynamics attributed to forest cover changes and CDHEs between Nanjing and Shaoguan from 2000 to 2022 to evaluate the impacts of human activities and climate change on forest carbon dynamics across different regions.

Table 1. The background of social, economic, and ecology in two regions.

Region	Climate	Main Land Type	Forest Cover Rate (2022)	GDP (2022)	Urbanization Rate (2022)
Nanjing	North Subtropical Monsoon	Farmland and Impervious Surface	25.86%	CNY 1.742 Trillion	86.8%
Shaoguan	Mid-Subtropical Monsoon	Forest	74.43%	CNY 0.162 Trillion	44.9%

Specifically, this research aims to (1) quantify the carbon budget due to forest cover change in two regions from 2000 to 2022 using CASA and bookkeeping models; (2) quantify the changes in forest carbon sequestration due to CDHEs in two regions from 2000 to 2022 using Geographical Detector and the photosynthesis equation; and (3) compare the difference in forest carbon dynamics caused by forest cover change and CDHEs in two regions during 2000–2022. For the first time, this study proposed an evaluation framework to illustrate the dynamic response of regional forest carbon to forest cover change and extreme climate events to determine the leading factors of forest carbon dynamics between the high economic and high forest cover regions and carry out targeted forest management and climate response policies according to regional characteristics.

2. Materials and Methods

2.1. Study Area

Nanjing (31°14′–32°37′ N, 118°22′–119°14′ E) and Shaoguan (23°53′–25°31′ N, 112°53′–114°45′ E) are both located in southern China, not only in geographical coordinates but also as critical economic and forestry hubs in Guangdong and Jiangsu Province (Figure 1). Shaoguan, for instance, boasts the wealthiest forest resources in Guangdong Province. However, it suffers from the adverse effects of climate change, rapid urban sprawl, and unscientific forestry management strategies, leading to a decline in forest cover and quality [32]. Human activities markedly influence the urban thermal environment of Nanjing, and the quantity of heat wave days has increased [33].

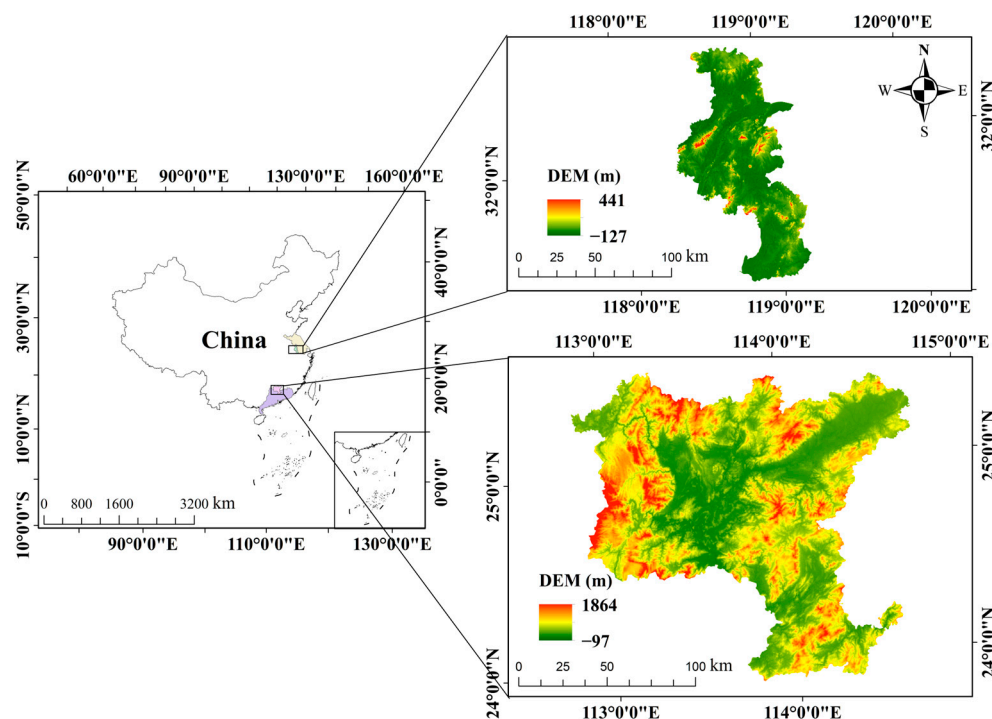


Figure 1. Locations of the study area. The background image shows the elevation in two regions based on the digital elevation model (DEM).

2.2. Data Sources and Processing

We used the Gap Filling and Savitzky–Golay filtering (GF-SG) method [34,35], synthesizing NDVI data from Landsat and MODIS products (Table 2) with a spatial resolution of 30 m. Meteorological data, including monthly average temperature, monthly total precipitation [36,37], and solar radiation data [38], were sourced from the Third Pole Environment Data Center (<http://data.tpsc.ac.cn>, accessed on 7 January 2024) (Table 2). Due to the lack of solar radiation data for 2022, the 2021 data are taken as the solar radiation data for 2022. We interpolated these datasets to a 30 m spatial resolution using Kriging and Inverse Distance Weighting (IDW) methods (Figure 2). We selected the first-order trend removal method to remove linear trends and used the Gaussian kernel function to implement Kriging interpolation. Meanwhile, we used the IDW of two power functions for interpolation, whose searching radius is 12 neighboring points. The land use/cover data were obtained from the annual China Land Cover Dataset (CLCD) (Table 2), which has a spatial resolution of 30 m [39]. The accuracy verification results based on 5463 independent reference samples show that the overall accuracy of the CLCD reaches 79.31% [39]. In Nanjing and Shaoguan, the main seven land types are farmland, forest, grassland, shrub, water, barren land, and impervious surface. We imported the processed data into the CASA model to obtain the study area's net primary productivity (NPP) from 2000 to 2022.

Table 2. Summary of datasets used in this study.

Dataset	Type	Selected Band	Resolution	Period
CLCD	Land Cover		30 m, Yearly [39]	2000–2022
Landsat 5 TM	NDVI	Band 3 and Band 4	30 m, 16-day	2000–2011
Landsat 7 ETM	NDVI	Band 3 and Band 4	30 m, 16-day	2012–2013
Landsat 8 OLI	NDVI	Band 5 and Band 4	30 m, 16-day	2014–2022
MOD09Q1	NDVI	Band 1 and Band 2	250 m, 8-day	2000–2022
Average Temperature	Temperature		0.833°, Monthly [36]	1901–2022
Total Precipitation	Precipitation		0.833°, Monthly [37]	1901–2022
Total Solar Radiation	Solar Radiation		2473 Stations [38]	1960–2021
Soil Type Distribution Data	Soil		1:1,000,000	1995

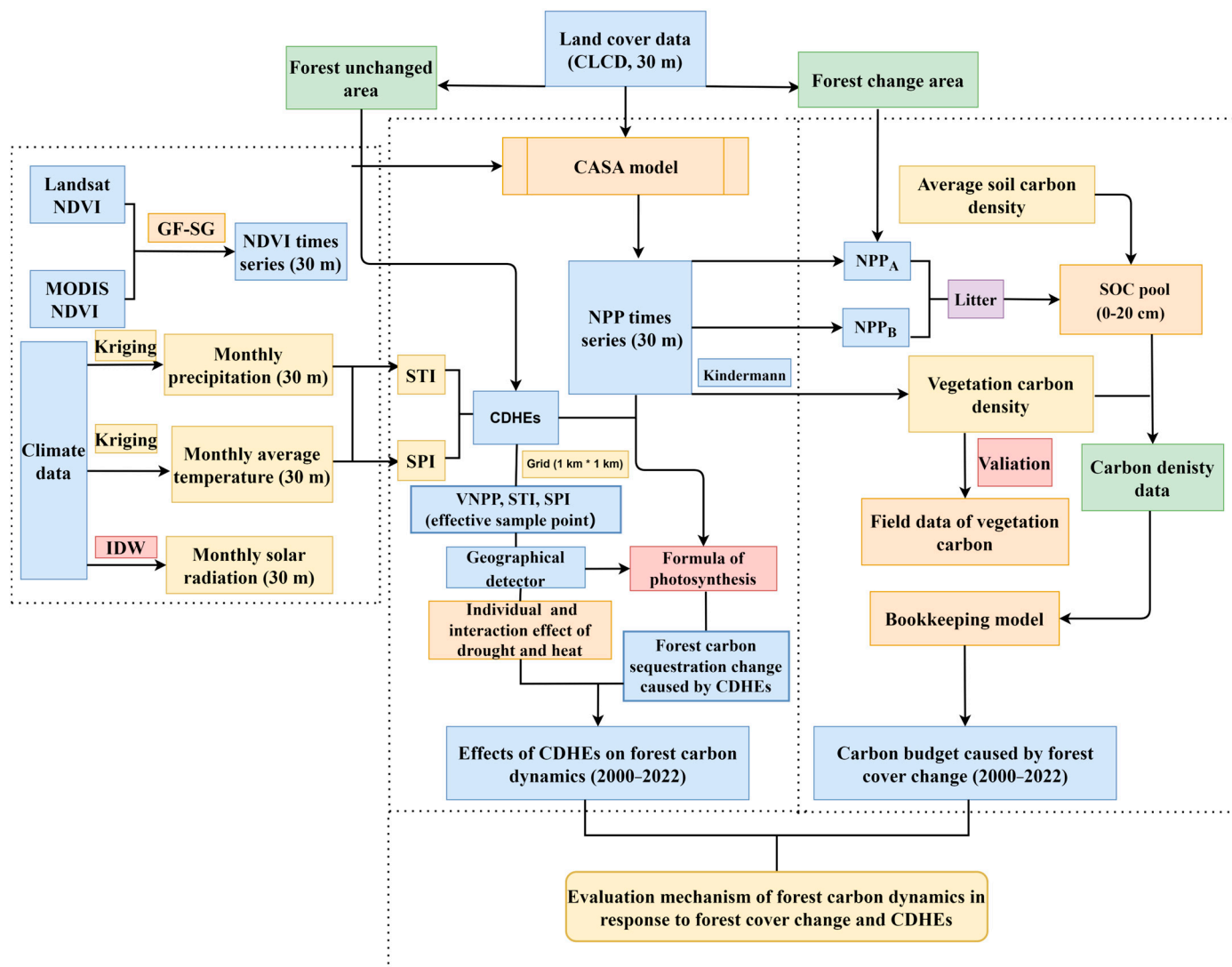


Figure 2. The workflow of this study.

Carbon density data were derived from land use/cover data, soil type distribution data, the literature, and field measurements. Soil type distribution data came from China's Second National Soil Survey (1:1,000,000), which we converted to a 30 m spatial resolution through vector-to-raster conversion. Vegetation average carbon density (Table S1) and soil average carbon density data (0–20 cm) (Table S2) were estimated from various literature sources [40–42]. To verify the accuracy of the CASA model in calculating carbon density, this research used forest sub-compartment survey data from the Guangdong Provincial Center for Forest Resources Monitoring, China, as validation data in the Shaoguan region in 2020 (Figure 2).

2.3. Impact of Forest Cover Change on Forest Carbon Dynamics

2.3.1. Inversion of NPP Data with 30 m High Spatial Resolution

Utilizing a refined CASA model [43–45], this study integrated processed meteorological data, the NDVI, and land use/cover data at a 30 m spatial resolution to estimate the net primary productivity (NPP) of Shaoguan and Nanjing. The model's output was primarily influenced by two parameters: photosynthetically active radiation and light energy use efficiency, which are critical factors in determining vegetation photosynthesis. Photosynthetically active radiation reflects the ability of vegetation to absorb solar radiation, while light energy use efficiency demonstrates the efficiency of vegetation in converting absorbed

light energy into organic matter. CASA models only need meteorological and land data to simulate and predict vegetation productivity at different times and spatial scales. This model's specific formula and principle are detailed in the paper of Zhu et al. [43].

2.3.2. Estimation of Vegetation Carbon Storage

Forest vegetation carbon density is typically calculated using the forest's average biomass and a carbon content coefficient of 0.5. We derived the average carbon density of forest vegetation based on the literature data (Table S1). Utilizing the positive linear relationship between forest biomass and NPP [46], we calculated the forest vegetation carbon density for each year in the study area, as shown in Equation (1). Combining these yearly forest vegetation carbon densities with the average vegetation carbon density data for other land types, we generated the vegetation carbon density data of the study area, with a spatial resolution of 30 m.

$$C_i = \frac{C_t \times N_i \times n_t}{\sum_{i \in t} N_i} \quad (1)$$

where i denotes a specific pixel; t represents the forest in a region; C_t represents the average forest carbon density in a region; N_i represents the net primary productivity of the pixel i ; C_i represents the vegetation carbon density of the pixel; n_t represents the total number of pixels occupied by the regional forest; and $\sum_{i \in t} N_i$ represents the total value of pixels of net primary productivity occupied by the regional forest.

2.3.3. Estimation of Soil Carbon Storage

The root–shoot ratio affects the distribution of the net primary productivity of above-ground and below-ground material [47]. All plant organs ultimately undergo senescence and enter the litter pool. Once in the soil, the litter produces carbon dioxide or forms organic matter. Each decomposition and transformation rate of litter is different due to the differences in the properties of litter, soil temperature, and moisture [48]. A fixed first-order decomposition rate was adopted to simplify the litter decomposition process. Based on the soil average carbon density (Table S2) and soil type distribution data, the product of litter productivity and turnover rate [31] was used to obtain the change in soil carbon density, as shown in Equations (2) and (3).

$$\Delta \text{Litter} = T_{AB} \cdot \sum_{i=1}^n \text{NPP}_{AB} \cdot (1 - T_{AB})^{n-i} + T_{BE} \cdot \sum_{i=1}^n \text{NPP}_{BE} \cdot (1 - T_{BE})^{n-i} \quad (2)$$

$$\Delta \text{SOC} = \Delta \text{Litter} \times T_L \quad (3)$$

where n represents the n th year of each cycle. ΔLitter denotes the total litter productivity in n year. NPP_{AB} represents above-ground NPP, while NPP_{BE} refers to below-ground NPP. T_{AB} and T_{BE} represent the rates of biomass turnover for above-ground and below-ground material. The ratio of NPP_{AB} to NPP_{BE} was estimated at 1:3 for grasslands and impervious surfaces. For forests and shrubs, the ratio is 1:4 [49,50]. The reap index of farmland is 0.3 [51]. The root turnover rate was also calculated as 0.15 per year for all vegetation types. The above-ground biomass turnover rate of the forest is 0.10 per year. Grasslands, farmlands, and impervious surfaces are 1.0 per year. T_L is the litter biomass turnover rate. The specific parameters are detailed in Cai et al. [52].

2.3.4. Bookkeeping Model

The bookkeeping model is extensively utilized to calculate the carbon budget by land use and cover change (LUCC). The model utilizes two types of data for its calculations: LUCC and carbon density. The model considers the total amount of carbon per unit area, including living organisms, soil, disturbed plant residues, and wood products [53]. This

model was used to calculate the carbon budget caused by forest cover change, as shown in Equation (4).

$$M = \sum_{n=1}^m \Delta SC_n + \Delta VC_n \quad (4)$$

where M denotes the carbon budget that arises from forest cover change; m represents the years of study; ΔSC_n denotes variations in soil carbon storage during the n th year; and ΔVC_n denotes variations in vegetation carbon storage during the n th year. ΔSC_n was calculated using Equation (5).

$$\Delta SC_n = \sum_{a=1}^m \sum_{b=1}^m \sum_{n=1}^m L_{a,b,n} \times \Delta SOC_{a,b,n} \quad (5)$$

where $L_{a,b,n}$ denotes the area where land type a was converted to b during the n th year; $\Delta SOC_{a,b,n}$ denotes the change in soil carbon storage where land type a was converted to b during the n th year.

The alterations in vegetation carbon storage resulting from forest cover change between 2000 and 2022 encompass two primary facets: the carbon dioxide emissions from deforested vegetation and the spontaneous regeneration of forest vegetation post-removal. Consequently, the vegetation carbon budget associated with these forest cover changes was computed based on Equation (6).

$$\Delta VC_n = \Delta VC_{RS} - \Delta VC_{RM} \quad (6)$$

where ΔVC_{RS} and ΔVC_{RM} signify the alterations in vegetation carbon storage that occur during the n th year as a result of recovery and vegetation removal, respectively. They can be calculated according to Equations (7) and (8).

$$\Delta VC_{RS} = \sum_{n=1}^m (L_{a,b,n} \times VD_a) \quad (7)$$

$$\Delta VC_{RM} = \sum_{a=1}^m \sum_{b=1}^m \sum_{n=1}^t L_{a,b,n} \times VD_a \times \alpha_k \times x_k \quad (8)$$

where α_k represents the proportion of vegetation carbon storage to total carbon storage at x_k oxidation rates; x_k represents the oxidation rate of removed vegetation in k forms; k denotes the oxidation forms of the removed vegetation, which include burning as fuelwood (within 1 year), paper oxidation (within 10 years), and the oxidation of building materials and furniture (within 100 years); and VD_a represents the vegetation carbon density of land type a . The bookkeeping model parameters (Table S3) were derived from Yang et al. [54].

2.4. Impact of Compound Drought and Heat Events on Forest Carbon Dynamics

2.4.1. Identification of Compound Drought and Heat Events

This study used monthly standardized precipitation index (SPI) and standardized temperature index (STI) data to identify CDHEs during 2000–2022 [55]. The principle of the SPI is to calculate the probability of Gamma distribution of precipitation in the specified period based on the total monthly precipitation, then carry out normalization processing, and finally use the standardized precipitation accumulation frequency distribution to classify the drought grade [56]. The SPI and STI were calculated following the same procedure. According to China's standardized precipitation drought grade, this study defines regions with an $SPI \leq -1.5$ as experiencing the occurrence of drought events. Similarly, we defined areas with an $STI \geq 1.5$ as experiencing the occurrence of heat events [57,58]. To alleviate the impacts of forest cover changes, we focused on the period from 2000 to 2022, during which forests were stable. During this time, we identified all occurrences of drought (heat) events and selected simultaneous events for combination ($SPI \leq -1.5$ and $STI \geq 1.5$). We termed this combination of two events CDHEs.

2.4.2. Identification of Carbon Dynamics

NPP is widely utilized in quantitatively analyzing vegetation carbon dynamics. We calculated the variation in NPP under CDHEs at a monthly scale, denoted as VNPP, serving as a short-term indicator of forest carbon dynamics, representing the increase or decrease in forest carbon sequestration efficiency. The forest vegetation displays a delayed response of 1–3 months to precipitation and temperature [59,60]. Therefore, we computed the forest VNPP response under CDHEs with lags ranging from one to three months according to Equations (9) and (10):

$$\text{VNPP}_0 = \text{NPP}_i - \text{NPP}_{i-1} \quad (9)$$

$$\text{VNPP}_m = \text{NPP}_{i+m} - \text{NPP}_i \quad (10)$$

where VNPP_0 denotes the change in forest NPP when forests do not exhibit a lagged response to CDHEs, i represents the year of occurrence of CDHEs, and VNPP_m signifies the change in forest carbon storage with a lag of m months under CDHEs. Furthermore, we conducted a correlation analysis between each drought (heat) event and forest VNPP to reflect the directional impact of drought (heat) events on carbon sequestration efficiency. Previous studies have suggested that human activities and climate change jointly influence forest carbon sequestration capacity [29,61]. Therefore, this study eliminated the disturbance of human activities on forest carbon dynamics by selecting unchanged forest vegetation. We utilized a created $1 \text{ km} \times 1 \text{ km}$ grid covering the study area to generate effective sampling points and extracted corresponding VNPP, SPI, and STI attribute values as spatial data sources for further analysis. We employed Pearson correlation tests and a 95% significance level test for statistical analysis. The SPI exhibited a positive spatial correlation with VNPP, indicating that VNPP decreases with increasing drought event intensity, suggesting a suppressive effect of drought events on carbon sequestration efficiency. The STI showed a negative spatial correlation with VNPP, indicating that VNPP decreases with increasing heat event intensity, also suggesting a suppressive effect of heat events on carbon sequestration efficiency.

2.4.3. Quantifying Single and Interactive Effects of CDHEs on Carbon Dynamics

GD is a statistical method to detect spatial differentiation and reveal the driving factors [17]. We used GD to analyze the effect of CDHEs on forest carbon dynamics quantitatively. GD requires discretizing input data; hence, discretizing drought (heat) events is necessary. We used the natural breakpoint method to divide the samples (SPI and STI) into seven categories (assigning these categories to 1–7, with a higher value indicating a higher intensity). We then imported these discrete SPI, STI, and VNPP data into GD for interpretation and interaction analysis. Next, an analysis of the explanatory power (q value) of the STI and SPI on VNPP and their interaction with VNPP was generated. The value of q ranges from 0 to 1. The larger the q value, the stronger the explanatory power. The principles of the model and related calculations are presented in paper [17]. Interaction detection in GD was used to identify the interactions between factors, i.e., to identify whether the effect of CDHEs on forest carbon dynamics would be stronger or weaker than that of single drought events (heat events) or whether the impact of drought events and heat events on forest carbon dynamics were independent of each other. The evaluation method involved comparing the single effect ($q(\text{drought})$, $q(\text{heat})$) and the interaction effect ($q(\text{drought} \cap \text{heat})$) based on q values (Table S4). Detailed evaluation criteria are shown in Table S4.

2.4.4. Quantifying Changes in Forest Carbon Sequestration Caused by CDHEs

Droughts and heat events change the amount of carbon sequestration in forests by affecting vegetation photosynthesis [12]. This study quantified the changes in forest carbon sequestration caused by CDHEs from 2000 to 2022. In addition, the delayed response of forests to drought and heat cannot be ignored. Therefore, using GD, this study obtained the optimal response time of forests to drought (heat) for CDHEs in the two regions during

2000–2022. We considered its maximum value as the duration of CDHEs and calculated the changes in forest NPP during this period. The change in forest NPP is calculated according to Equation (11):

$$NPP_C = \sum_{A=i}^{i+n} NPP_A - \sum_{B=i}^{i+n} NPP_B \tag{11}$$

where NPP_C represents the change in forest NPP caused by CDHEs; NPP_A represents the NPP during the period from the occurrence to the optimal lag time of the CDHEs; NPP_B represents the average NPP in the same period during which no CDHEs occurred; i represents the month when CDHEs occurred; and n represents the month of the optimal response time. Then, the chemical formula of vegetation photosynthesis, $6CO_2 + 6H_2O - C_6H_{12}O_6 + 6O_2$, was used to calculate the forest carbon sequestration change caused by CDHEs [29]. The forest carbon sequestration change was calculated according to Equation (12):

$$C_{FSC} = \frac{NPP_C}{0.45} \times 1.62 \tag{12}$$

where C_{FSC} represents the amount of forest carbon sequestration change caused by CDHEs.

3. Results

3.1. Effects of Forest Cover Change on Forest Carbon Dynamics

3.1.1. Spatiotemporal Dynamics of Primary Land Area Change from 2000 to 2022

CLCD-based main land type area change from 2000 to 2022 was estimated. As shown in Figure 3, we found that forest is the primary land use type in Shaoguan, and its impervious surface area takes up a small proportion. In Nanjing, farmland and impervious surfaces are the primary land types, and their area is larger than forests. From 2000 to 2022, the area of forest and farmland in Nanjing decreased by 9040.6 ha and 61,746.9 ha, respectively. In contrast, the areas of impervious surfaces increased significantly by 71,143.2 ha (Figure 3). The forest area in Shaoguan decreased by 59,049.9 ha. In contrast, the areas of farmland and impervious surfaces increased by 46,946.6 ha and 13,868.5 ha, respectively.

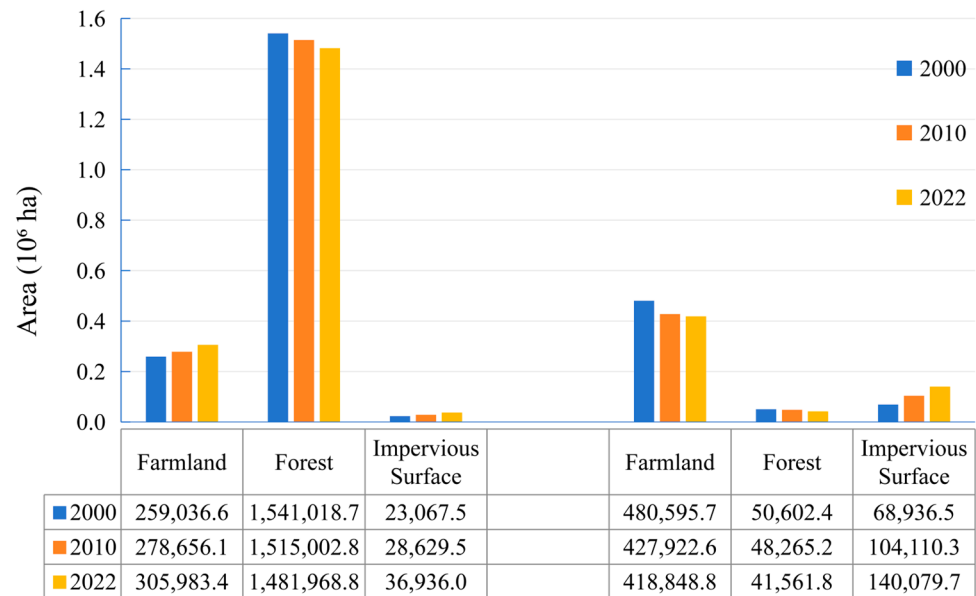


Figure 3. Area of main land use types in Nanjing and Shaoguan from 2000 to 2022 (unit: ha).

3.1.2. CASA Model Performance

To assess the precision of vegetation carbon density estimates obtained from the CASA model, we compared these estimates with field-observed forest vegetation carbon density data acquired from forest sub-compartments of Shaoguan in 2020. This demonstrated a notable correlation between the vegetation carbon density originating from the CASA

model's NPP results and the sub-compartment survey carbon density values, with an R^2 of 0.64 (Figure 4). This suggested that the vegetation carbon density estimated from the CASA model's NPP results had a good fit and high correlation with the field-measured vegetation carbon density values, confirming that the CASA model-derived vegetation carbon density values were suitable for subsequent analysis.

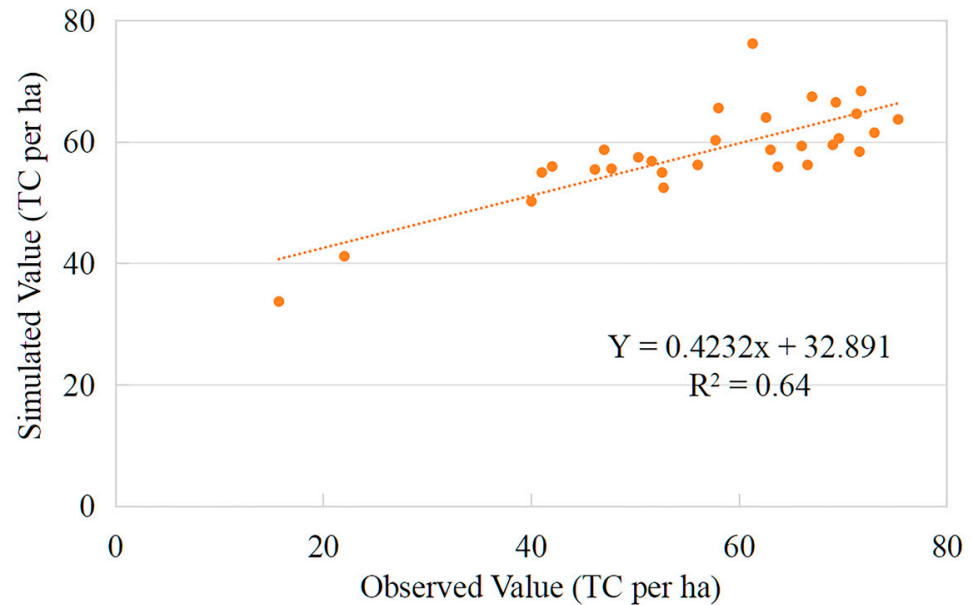


Figure 4. Comparison between simulated and observed forest carbon density in Shaoguan, 2020.

3.1.3. Forest Cover Change in Different Regions and Its Resulting Carbon Budget

The study area's forest cover change from 2000 to 2022 was estimated using the CLCD. Figures 5 and 6 indicate significant forest cover change. The forest area of Nanjing and Shaoguan showed a decreasing trend. The main reason for the decrease in forest area in the two cities is the conversion of forest into farmland. They had 93.8% and 96.6% of the forest loss area, respectively (Tables S5 and S6). However, they differed in the trend in forest cover change types and regions. For example, the farmland returned to forest in Shaoguan showed an increasing trend, while the farmland returned to forest in Nanjing showed a decreasing trend (Tables S5 and S6).

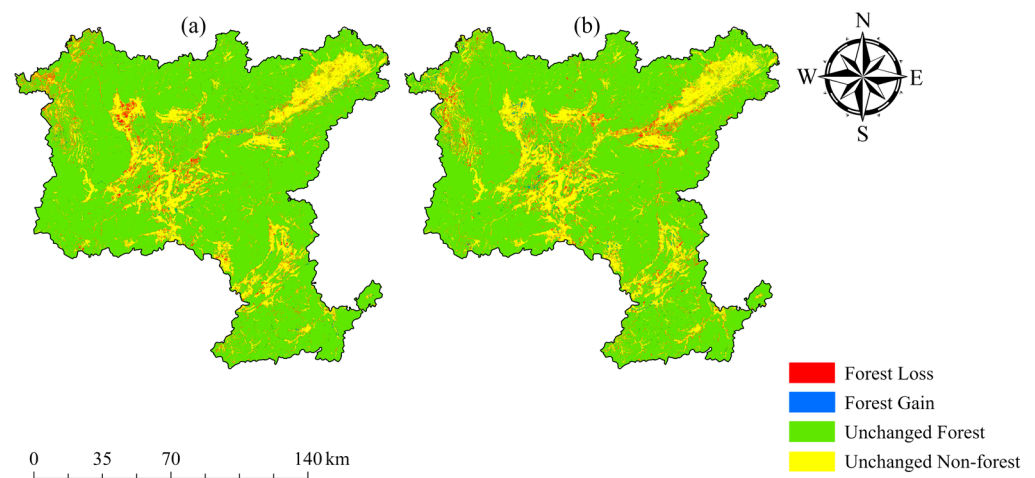


Figure 5. Forest cover change in Shaoguan from 2000 to 2010 (a) and 2010 to 2022 (b).

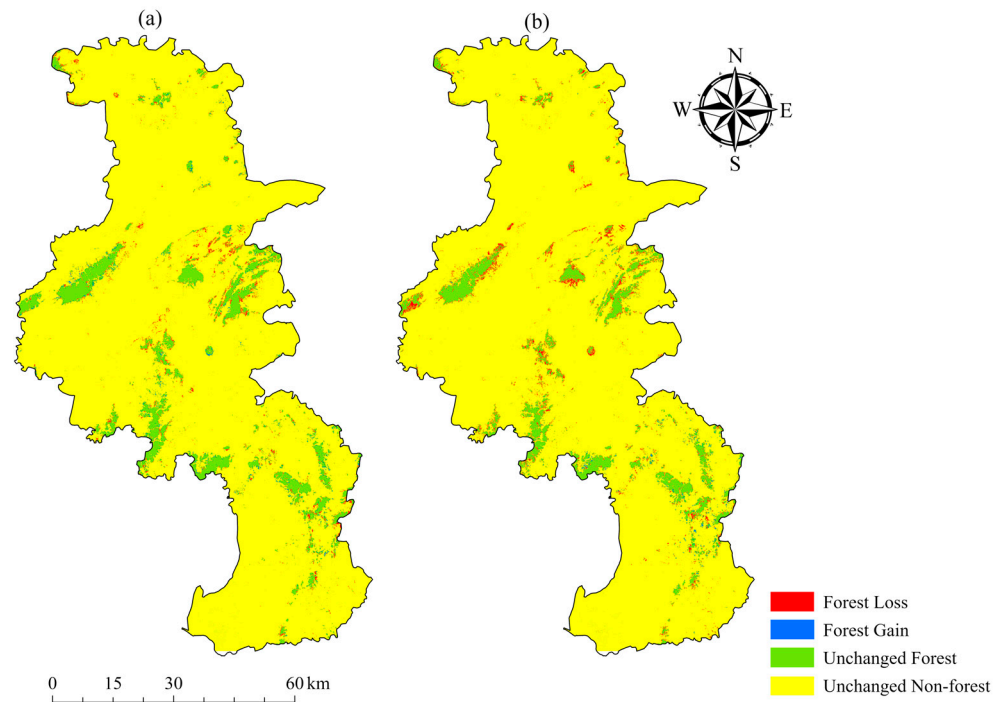


Figure 6. Forest cover change in Nanjing from 2000 to 2010 (a) and 2010 to 2022 (b).

Combining CASA with the bookkeeping model, we obtained the carbon budget caused by forest cover change in the two regions (Figure 7). The two regions’ carbon flux caused by forest cover change showed significant spatial differences. The carbon flux in Shaoguan was predominantly observed in the western, central, northeastern, and southern zones, exhibiting a relatively dense pattern. Specifically, the carbon flux was primarily manifested as carbon loss in the west and central areas. The northeast region showed carbon sequestration. In the southern region, both carbon loss and carbon sequestration were present. Nanjing’s central and southern areas are concentrated areas of carbon flux caused by forest cover change. The carbon flux in the central region was mostly carbon loss, while that in the south region was carbon sequestration.

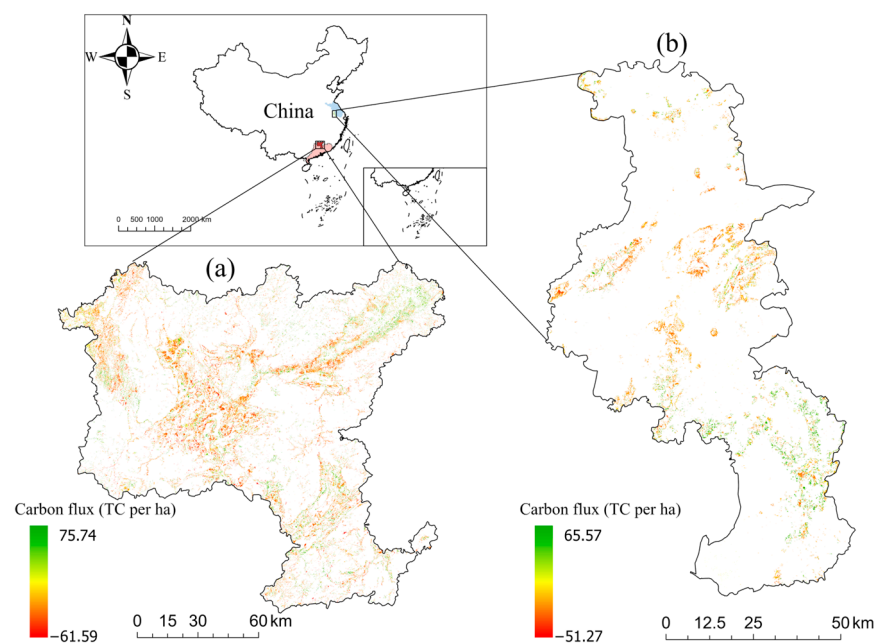


Figure 7. Carbon storage change between 2000 and 2022 in Shaoguan (a) and Nanjing (b).

To study the carbon flux caused by different types of forest cover change, we identified two land use patterns based on forest cover change: afforestation and deforestation (Table S7). Figure 8 shows that afforestation in the two regions led to a net carbon accumulation in vegetation biomass and soil, increasing forest carbon storage by 0.269 TgC in Nanjing and 1.509 TgC in Shaoguan from 2000 to 2022. The total carbon loss caused by deforestation was 0.491 TgC in Nanjing and 2.802 TgC in Shaoguan. The results showed that afforestation increased forest carbon storage, while deforestation caused forest carbon loss. The deforestation area was much larger than the afforestation area in both regions, and the carbon budget caused by forest cover change showed a net carbon loss, with 1.293 TgC in Shaoguan and 0.222 TgC in Nanjing from 2000 to 2022.

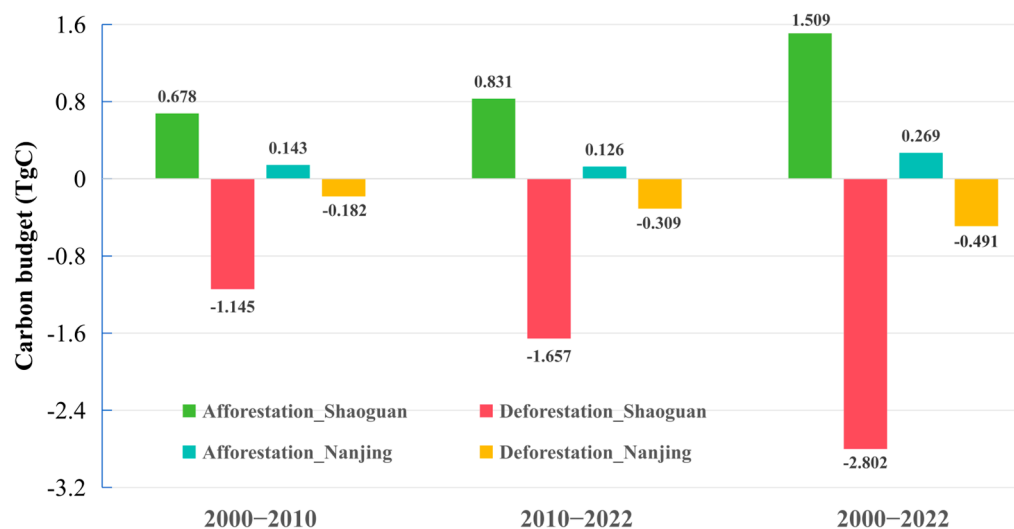


Figure 8. The carbon budget caused by changes in forest cover types in the two regions from 2000 to 2022.

3.2. Effects of CDHEs on Forest Carbon Dynamics

3.2.1. Spatial Distribution of CDHEs

Using the monthly SPI and STI, we pinpointed drought and heat occurrences during the vegetation growth period from 2000 to 2022. Drought events occurred for 13 months, and heat events for 21 months. We then identified three CDHEs during 2000–2022 in each region (Figures 9 and 10). Most CDHEs in the two regions occurred between July and September (Figure S1). Nanjing and Shaoguan have frequent summer and autumn heat in southern China. The geographical spread of drought exhibited more significant variability than heat. Furthermore, variations in the intensity of drought and heat were observed across different CDHEs within the same region. We found the highest intensity and coverage of CDHEs in July 2003 and August 2022 in Shaoguan and Nanjing, respectively (Figure S1).

3.2.2. Impact of Drought and Heat Events on Forest Carbon Dynamics in Different Regions

Figure 11 shows the effects of drought and heat events on forest carbon dynamics in the two regions, with the CDHEs occurring during 2000–2022. The single-factor average explanatory power (q value) of the heat events in September 2021 in the Shaoguan region was only 0.101, which was lower than that of the drought events (0.110) (Figure 11). The average explanatory power (q value) of the heat events (0.112) was greater than that of drought events (0.109) during 2000–2022. This indicated that heat events substantially impacted forest carbon dynamics in Shaoguan compared to drought events.

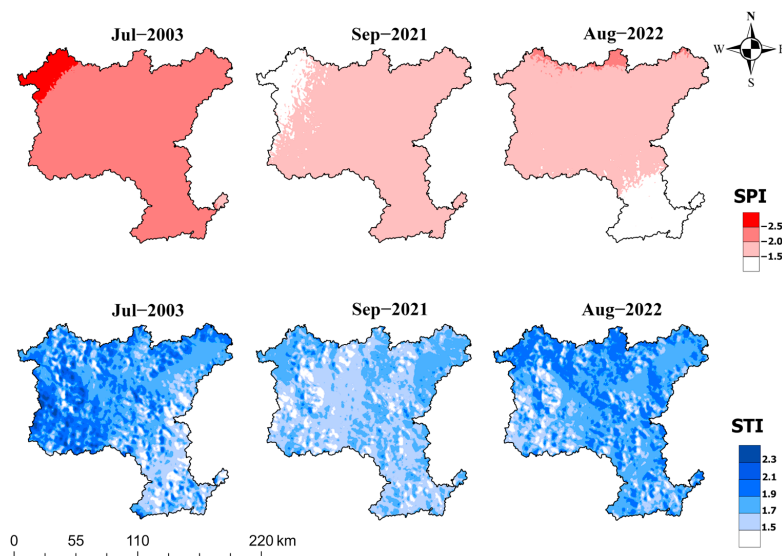


Figure 9. Spatiotemporal patterns of drought and heat events in Shaoguan from 2000 to 2022.

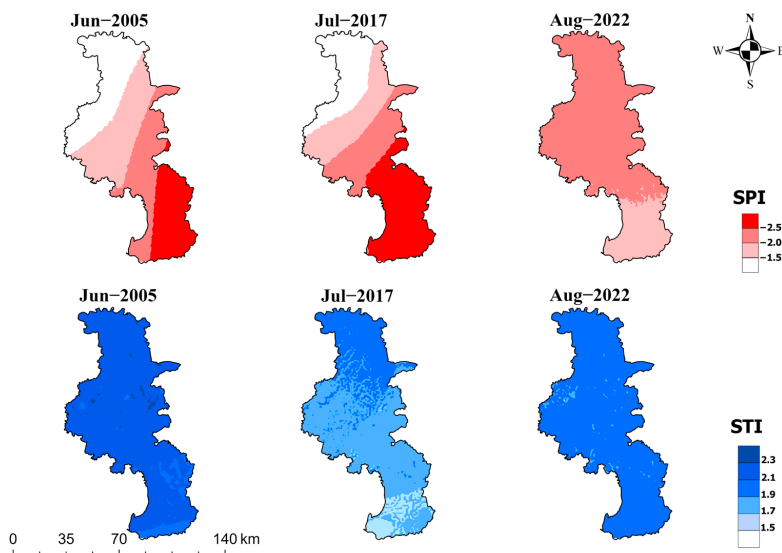


Figure 10. Spatiotemporal patterns of drought and heat events in Nanjing from 2000 to 2022.

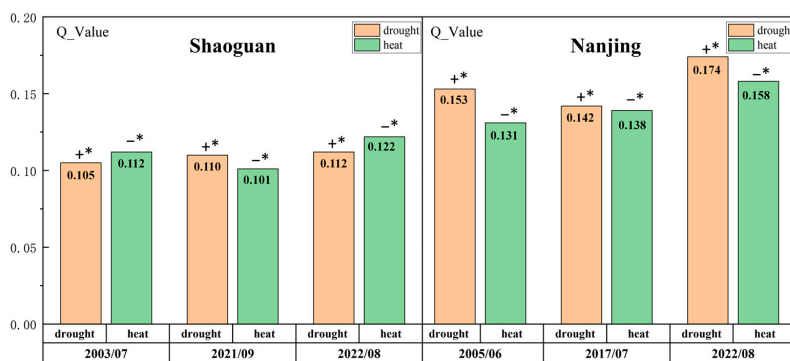


Figure 11. The q value of the impacts of drought and heat events on VNPP in Nanjing and Shaoguan. Note: + indicates that drought (heat) events are positively correlated with VNPP and – indicates that drought (heat) events are negatively correlated with VNPP; * suggests that the 95% significance test is passed.

Based on three instances of CDHEs in Nanjing, the q value of the impacts of the heat events on forest carbon sinks was smaller than that of drought events. The average q

value of the effects of the heat events on forest carbon sinks during 2000–2022 was 0.142, which was lower than that of drought events (0.156). This indicated that drought events significantly impacted forest carbon dynamics more than heat events in Nanjing.

The correlation analysis between the drought (heat) event index and VNPP in CDHEs of the two regions from 2000 to 2022 pointed out that the drought events were positively correlated with VNPP, while the heat events were negatively correlated with VNPP (Figure 11). The more severe the drought (heat) event, the smaller the VNPP, and the lower the forest carbon sink capacity. Overall, drought and heat events affected forest carbon dynamics by inhibiting forest carbon sink capacity.

3.2.3. Delayed Effects of Drought and Heat Events on Forest Carbon Sequestration

We used GD to calculate the effects of drought (heat) events on short-term forest carbon sequestration capacity (VNPP) in three CDHEs in each of the two regions and obtained their average q value with a lag of one, two, and three months (Table 3). It was evident that the maximum average q value of the effects of drought events on forests was 0.129 for Shaoguan and 0.174 for Nanjing, while heat events exhibited q values of 0.149 and 0.169. This suggested a delay in the impact of drought and heat events on forests in these two regions, with a lag time of two months.

Table 3. Lagged effects of drought and heat events in Nanjing and Shaoguan.

Region	q	No Lag	1-Month Lag	2-Month Lag	3-Month Lag
Nanjing	q (drought)	0.140	0.147	0.174	0.165
	q (heat)	0.112	0.140	0.169	0.149
Shaoguan	q (drought)	0.083	0.106	0.129	0.118
	q (heat)	0.089	0.098	0.149	0.111

3.2.4. Impact of CDHEs on Forest Carbon Dynamics

Based on GD, we found that the average interaction impacts of CDHEs on forest carbon sequestration efficiency in Shaoguan and Nanjing were 0.224 and 0.318, respectively (Table 4). These q values were notably above the average ones observed for single events (0.109 and 0.112 for Shaoguan; 0.156 and 0.142 for Nanjing, Figure 11). The impacts of CDHEs on VNPP showed bi-factor-enhanced or nonlinear-enhanced modes. For example, CDHEs in Shaoguan (q (drought \cap heat) = 0.206) (Table 4) had a more significant impact on forests compared to the single effects of drought (q (drought) = 0.110) and heat (q (heat) = 0.101) in 2021 (Figure 11), with the interaction showing a synergistic enhancement. CDHEs in Nanjing (q (drought \cap heat) = 0.361) had a more significant impact on forests compared to the single effects of drought (q (drought) = 0.174) and heat (q (heat) = 0.158) in 2022 (Figure 11), with the interaction displaying a nonlinear synergistic enhancement.

Table 4. Interaction modes of the impacts of different drought and heat events on carbon dynamics.

Year/Month	Interaction Modes	Nanjing	Shaoguan
2003/07	D \cap H		0.225 ∇
2005/06	D \cap H	0.298 ∇	
2017/07	D \cap H	0.294 ∇	
2021/09	D \cap H		0.206 \diamond
2022/08	D \cap H	0.361 ∇	0.242 ∇
Average		0.318	0.224

Note: ∇ represents a nonlinear-enhanced mode; \diamond represents a bi-factor-enhanced mode.

3.2.5. Forest Carbon Sequestration Change Caused by CDHEs

The overall effect of CDHEs on the change in carbon sequestration in the two regions was manifested as net carbon loss. In Table 5, the CDHEs in Nanjing caused the most significant carbon loss (−0.0844 TgC) in August 2022 and the most minor (−0.0374 TgC) in June 2005. The CDHEs in Shaoguan caused the most significant carbon loss (−1.456 TgC) in July 2003 and the most minor (−0.705 TgC) in September 2021. Overall, CDHEs in Shaoguan caused

a total carbon loss of -3.219 TgC, much more significant than that in Nanjing (-0.186 TgC) during 2000–2022. Based on Figure 9, Figure 10, and Figure S1, we found that the higher the intensity of CDHEs, the greater the forest carbon loss.

Table 5. Forest carbon loss caused by CDHEs in two regions (unit: TgC).

Year/Month	Nanjing	Shaoguan
2003/07		−1.456
2005/06	−0.0374	
2017/07	−0.0645	
2021/09		−0.705
2022/08	−0.0844	−1.058
Total carbon loss	−0.186	−3.219

3.3. Comparisons Between the Impacts of Forest Cover Change and CDHEs on Forest Carbon Dynamics

In Nanjing, the net carbon loss caused by forest cover change (0.222 TgC) was more significant than that caused by CDHEs (0.186 TgC) during 2000–2022, indicating that the carbon loss caused by forest in Nanjing was dominated by human activities (Figure 12). Conversely, the net carbon loss caused by forest cover change in Shaoguan (1.293 TgC) was smaller than that caused by CDHEs (3.219 TgC), indicating that extreme climate was the dominant factor causing forest carbon loss in Shaoguan. Both factors caused the most forest carbon loss in Shaoguan, especially CDHEs. The effects of CDHEs and forest cover change on forest carbon dynamics had two sides. Afforestation can increase forest carbon storage, while deforestation can cause forest carbon emissions. Moderate heat events caused an increased photosynthesis effect, increasing forest carbon sequestration capacity and forest carbon storage. In contrast, extreme heat and drought affected vegetation photosynthesis and even led to vegetation death, decreasing forest carbon storage. However, there are differences in how forest cover change and CDHEs affect forest carbon dynamics. Forest cover change directly led to the decrease or increase in forest carbon storage through the decrease or increase in forest area. The carbon loss caused by CDHEs was mainly due to the decrease in forest carbon sink capacity.

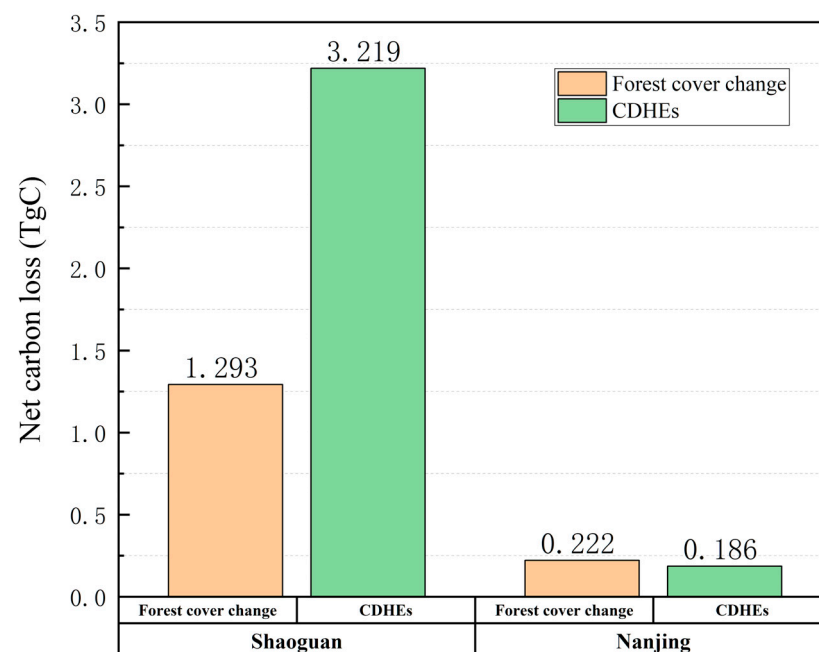


Figure 12. Forest cover change and CDHEs caused net carbon loss in the two regions during 2000–2022.

4. Discussion

4.1. Impact of Forest Cover Change on Carbon Dynamics

The bookkeeping model effectively estimates carbon stocks and fluxes resulting from LUCC [9,53]. Although it is extensively utilized for national and global carbon estimations, it faces challenges when applied to regional scales with spatially detailed carbon accounting. To address this limitation, we combined the bookkeeping model with the CASA model, utilizing the linear relationship between forest NPP and forest biomass to estimate forest vegetation carbon density. Furthermore, we integrated literature-based carbon density for diverse vegetation and soil categories into the carbon accounting process, generating spatially detailed carbon flux data. This approach enables the monitoring of forest carbon dynamics under forest cover changes at fine scales in Shaoguan and Nanjing.

Using the bookkeeping model in Nanjing and Shaoguan, we estimated the carbon fluxes resulting from forest cover changes from 2000 to 2022. The spatial distribution map of carbon flux (Figure 7) and statistical map (Figure 8) show that the carbon budget caused by forest cover change is similar and different in both regions. The similarity is that the forest area of Nanjing and Shaoguan decreased significantly during 2000–2022, which is consistent with the conclusion of Zhao et al. [32]. The decreased forest area indicated that the afforestation area is lower than deforestation's. Therefore, carbon emissions caused by forest cover change exceeded carbon sequestration in Nanjing and Shaoguan during the study period, resulting in net carbon loss. This is consistent with previous research results [62–64]. However, there is a significant difference in the resulting net carbon loss between the Shaoguan and Nanjing regions between 2000 and 2022. The net carbon loss in Shaoguan was 1.293 TgC. In contrast, the net carbon loss from forests in Nanjing was only 0.222 TgC. The main reason for this difference is that the forest area of Shaoguan has been reduced more than Nanjing's.

The carbon flux caused by afforestation in Nanjing is mainly concentrated in the central and southern areas of Nanjing. The carbon fluxes caused by afforestation in Shaoguan were focused on the central, northeastern, northwestern, and southern regions. This is supported by the data on afforestation distribution in the Chinese Forestry Statistical Yearbook [65] (<http://202.99.63.178/c/www/tjnj.jhtml>, <https://cnki.nbsti.net/CSYDMirror/trade/Yearbook/Single/N2006050899?z=Z010>, accessed on 14 March 2024). At the same time, we found that the carbon loss was mainly concentrated in the central part of Shaoguan and the central part of Nanjing. These regions are near farmland, indicating that expansion mostly led to deforestation. This suggests that human activities mainly dominate the change in forest cover in the two regions. However, according to Figure 3, the farmland area in Nanjing did not increase but declined, while the farmland area in Shaoguan showed an increasing trend. This showed that the two regions' factors driving forest conversion to farmland differ. This phenomenon may be due to policy differences in the different areas. Since the early 21st century, Shaoguan has upgraded the scale and quality of its cultivated land to promote agricultural development. At the same time, Nanjing has strengthened its Yangtze River protection policy during the urbanization process, focusing on afforestation and forest protection [66]. In the meantime, Nanjing's urban expansion took up a lot of farmland. Nanjing needs to reduce the area of forests converted into farmland to maintain food security [67]. It also inhibited the afforestation area to a certain extent. As a result, the afforestation area in Nanjing showed a declining trend.

Indeed, we emphasized the need for equal attention and careful assessment of the potential negative impacts of deforestation on forest carbon stocks in enhancing forest carbon stocks through the expansion of afforestation areas. Not only does deforestation contribute to global climate change by releasing stored carbon back into the atmosphere, but it can also undermine ecosystem integrity and biodiversity, with long-term adverse effects on the overall carbon sink function of forests [68,69]. Therefore, when developing and implementing afforestation and forest management strategies, the double-sided impact of afforestation and deforestation should be comprehensively considered to ensure that the

trend in deforestation is effectively contained and reversed while forest carbon storage is increased to maintain the positive role of forests as an essential carbon sink of the earth [70].

4.2. Impact of CDHEs on Carbon Dynamics

We utilized the interaction module of GD to assess the precise effect of CDHEs on forest carbon dynamics. The results indicated that CDHEs had reduced forest NPP, inhibiting forest carbon sequestration efficiency. This finding aligned with conclusions from Li et al. [12], Zhao et al. [11], and Wang et al. [30]. Qu et al. [2] demonstrated that extreme drought and heat negatively impact vegetation carbon fluxes and ecosystem productivity. When temperatures exceed the tolerance range of vegetation, enzyme denaturation may accelerate, thereby suppressing growth [2,71,72]. Drought reduced carbon sequestration capacity by affecting ecosystem photosynthesis and respiration, fundamentally altering the functionality and structure of terrestrial ecosystems and potentially transforming them into carbon sources [2,73].

Our study found that drought events more significantly explained the carbon dynamics in Nanjing forests than heat events. In contrast, heat events played a more significant role in carbon dynamics in Shaoguan. This variability may stem from the complexity of environmental factors affecting vegetation photosynthesis during CDHEs. Differences in study scope, duration, and modeling approaches contribute to varying assessments of the impact of heat and drought on VNPP. Some studies have emphasized that latitude is an essential factor that should not be ignored in assessing global or regional CDHEs [74]. This is due to the amount of heat the sun radiates at different latitudes, complicating the correlation between CDHEs. There is a difference in latitude between Nanjing and Shaoguan. This regional thermal difference further leads to differences in the ability of forest ecosystems at different latitudes to adapt to CDHEs [74].

We observed a two-month lagged effect of drought and heat events on forest vegetation types, indicating that forests have a specific capacity for recovery from extreme weather conditions. This finding aligns with previous research results [75,76]. Forest vegetation has efficient water regulation mechanisms, flexible leaf stomatal control, and strong water absorption from deep root systems [12]. Li et al. [12] suggested that vegetation may adjust parameters such as photosynthetic rate and water use efficiency in reaction to environmental pressures following extreme climate events, potentially leading to delayed forest responses. Therefore, it shows resistance in the face of CDHEs.

Table 4 indicates that CDHEs have a more substantial impact on forest NPP than single extreme events. Previous studies showed that heat can trigger heat stress in vegetation, which damages photosynthetic enzymes and inhibits the process of photosynthesis. When drought coincides with heat, it creates a low-humidity environment that exacerbates the adverse effects of heat stress and further reduces the trend of decreasing photosynthetic efficiency [12,77]. This study revealed a pattern of synergistic or nonlinear enhancement of CDHEs, suggesting that CDHEs have a more severe impact on forest carbon dynamics than a single event, consistent with prior research findings [2,78]. The results emphasized the importance of quantifying the effects of CDHEs on forest carbon dynamics. Finally, using the photosynthesis equation and the optimal response time, we obtained the change in forest carbon sequestration due to each CDHE in the two regions. The results show that CDHEs lead to a decrease in forest carbon sequestration. With the increase in the intensity of CDHEs, the reduction in forest carbon sequestration also increased.

Therefore, in the context of global warming, increased attention must be paid to CDHEs to enhance the carbon sequestration potential of forest ecosystems. We should develop targeted coping strategies based on forests in different regions. For example, adjusting the planting structure of some forest vegetation, as well as timely irrigation and fertilization, will enhance the adaptability of forests to CDHEs. At the same time, forests have demonstrated resistance to CDHEs. This discovery has prompted us to develop more ecosystem conservation and management strategies, especially in ecologically vulnerable

areas. The adverse impacts of CDHEs on ecosystems can be mitigated by adopting strategies such as reforestation and fallowing [12].

4.3. Differentiated Impacts of Forest Cover Change and CDHEs on Forest Carbon Dynamics

The net carbon loss due to CDHEs and forest cover changes between 2000 and 2022 showed significant differences in the two regions. The discrepancy might be attributed to variations in city types. Urbanization would directly affect the forest's carbon storage [79]. Xu et al. [80] believed that urban expansion caused by urbanization causes the removal of forest vegetation, and the carbon absorption capacity of carbon sinks rapidly declines. At the same time, China is undergoing a rapid urbanization process with low vegetation coverage, and large areas of forest vegetation are cleared to meet the needs of urban population growth and economic development. As a significant financial center city in the Yangtze River Delta region, Nanjing's urbanization process is higher [81]. With the deepening of this process, the population of Nanjing has shown a sharp growth trend [81]. The surge in population is placing higher demands on food supplies, which in turn is driving the demand for farmland of a specific size. In this context, the land use pattern in the Nanjing area has changed significantly, especially since the conversion of forest to farmland has become frequent [82]. Therefore, the intensification of urbanization in Nanjing significantly impacts forest carbon storage through population growth and land use patterns. This also explains why forest cover change has become the main factor leading to forest carbon loss in Nanjing. This is consistent with Chuai et al.'s [83] belief that urban sprawl is the leading cause of carbon emissions in the eastern seaboard.

Shaoguan, as a typical forest city in Guangdong Province, has a low urbanization level and a high forest cover. Human activity is relatively minimal. China has rolled out a series of policies aimed at ecological conservation in the south, such as the South China Timber Production Plan, which somewhat offset the carbon loss caused by forest cover change in Shaoguan [84]. Shaoguan is in the northern region of Guangdong, south of the Nanling Mountains. The Nanling Mountains block precipitation formation, partly leading to drought. Additionally, the karst geology in the northern Guangdong region exhibits significant ecological fragility, frequently encountering problems of soil and water loss [85,86]. This unique geological structure lacks good water storage and precipitation replenishment capabilities, which may reduce surface water flow and limit evaporation during the growth process of young forests and artificial forests. This also helps explain why forest carbon loss in the Shaoguan area is mainly affected by CDHEs. It should be noted that there is a strong link between deforestation in low latitudes and climate warming [87,88]. Global warming has further promoted the frequent occurrence of CDHEs, forming a vicious circle [89]. It is suggested that the importance of forest cover changes together with CDHEs in low-latitude regions needs to be considered.

Forest management policies should be developed for different urbanization levels and geological conditions [90]. In highly urbanized areas, supervision of land use change should be strengthened to prevent forest carbon loss caused by overdevelopment [91]. In areas with high forest coverage, the control of human disturbance should be strengthened to reduce forest carbon loss. We will improve the protection of ecologically fragile areas to prevent soil erosion and ecological degradation [92,93].

4.4. Uncertainties and Future Works

On the one hand, we combined the bookkeeping model with the CASA model to achieve spatially detailed carbon budget estimates due to forest cover change [9,25]. Experimental intervals of 10 and 12 years were used to simplify forest cover change in the model. However, due to uncertainties in predicting when transitions occur, there is a possibility of overestimating the duration of forest cover change, leading to increased carbon budgets [31]. At the same time, the input data of the CASA model include the remote sensing vegetation index, air image data, land cover data, and so on [94]. These data's quality, resolution, and spatiotemporal coverage affect the model's accuracy [94]. The bookkeeping

model parameters do not fully represent vegetation across an entire climatic zone [9]. This involves the accuracy of the model and the uncertainty of the experimental results to some extent.

On the other hand, we quantified the response of forest carbon dynamics to CDHEs using GD and the photosynthesis equation [13,29]. This provided new insights into the influence of CDHEs on forest carbon dynamics. However, the spatial scale of meteorological data was relatively coarse, and small-scale spatial resolution meteorological data were mostly obtained through interpolation methods, which led to a certain degree of error in the accuracy of the meteorological data. Hence, incorporating higher-resolution meteorological datasets into future research can significantly enhance data accuracy. In addition, this research used monthly time scale results, mainly focusing on the short-term effects of CDHEs on forests. At the same time, this study also considers the delayed response of forests to drought (heat) events and vegetation [30]. The cumulative effects of drought and heat events on forest carbon fixation were ignored. Furthermore, we lacked specific experimental studies to explore the biophysical and biochemical mechanisms underlying regional differences in forest carbon dynamics, especially those closely related to key environmental variables such as soil properties, water status, and water availability.

Future studies should reduce the experimental interval to ensure that forest cover changes can be captured in the short term to more accurately assess the process and influencing factors of the forest carbon cycle. Given the parameter accuracy of the CASA and bookkeeping models, we should focus on optimizing model parameter settings. By introducing higher-quality datasets to improve the prediction accuracy and reliability of the models, we can ensure that the meteorological data can more genuinely reflect the actual state of the forest ecosystem. Finally, because of the lack of discussion on the dynamic influencing mechanism of forest carbon in different regions in current studies, we should focus on soil characteristics, water status, climate change, human activities, and other factors and thoroughly analyze how these factors affect the storage, absorption, and release of forest carbon through field observation, experimental operation, model simulation, and other means. And the mechanism of their interaction should also be studied. At the same time, we will supplement the cumulative effect of extreme weather events on forest carbon dynamics [13,95].

5. Conclusions

In this study, the bookkeeping and CASA models were combined to quantify the carbon budget caused by forest cover change, and the forest carbon sequestration change caused by CDHEs was estimated using GD and photosynthesis equations. The forest carbon dynamics caused by forest cover change and CDHEs in the two regions were comprehensively compared. On the one hand, forest cover change in both cities resulted in net forest carbon loss. The net carbon loss caused by forest cover change was 0.222 TgC and 1.293 TgC in Nanjing and Shaoguan, respectively. On the other hand, drought and heat events inhibited the efficiency of forest carbon sequestration. Forest carbon sinks showed a typical two-month lag response to drought (heat) events. The effect of CDHEs on forest carbon sinks is more significant than that of single extreme events, showing nonlinear enhancement and a two-factor interaction mode. We found that CDHEs dominated forest carbon loss in Shaoguan. CDHEs caused a net carbon loss of 0.186 TgC and 3.219 TgC in Nanjing and Shaoguan, respectively. In Nanjing, forest cover change dominated the forest carbon loss. CDHEs dominated forest carbon loss in Shaoguan. This study provided an evaluation framework for quantifying the effects of forest cover change and CDHEs on forest carbon dynamics. This finding contributes to a deeper understanding of the mechanisms of climate change's impact on forest carbon sinks. It shows that relevant departments need to consider the effects of forest cover change and extreme climate events to protect and enhance the carbon sink function of forests more effectively.

Supplementary Materials: The following supporting information can be downloaded at <https://www.mdpi.com/article/10.3390/f15112048/s1>, Table S1: Vegetation carbon density (unit: TC per ha); Table S2: Soil carbon density (0–20 cm, unit: TC per ha); Table S3: Parameters of bookkeeping model; Table S4: Interaction between explanatory variables; Table S5: Forest cover change area in Shaoguan City from 2000 to 2022 (unit: ha); Table S6: Forest cover change area in Nanjing City from 2000 to 2022 (unit: ha); Table S7: Forest cover change type; Figure S1: Spatial distribution of combined drought and heat events (CDHEs) in Shaoguan (a) and Nanjing (b).

Author Contributions: C.G.: writing—original draft. T.W.: validation. W.S.: writing—review and editing, supervision, and conceptualization. Z.T.: investigation. X.S.: investigation. J.H.: writing—review and editing and data curation. T.H.: resources. W.G.: methodology. C.H.: conceptualization. All authors have read and agreed to the published version of the manuscript.

Funding: Our work was jointly funded or supported by the National Natural Science Foundation of China (32371878, 32001251), the Youth Science and Technology Talent Lifting Project of Jiangsu Province, the Natural Science Foundation of Jiangsu Province (BK20200781), and the Priority Academic Program Development of Jiangsu Higher Education Institutions (PAPD). Special thanks to the Guangdong Provincial Center for Forest Resources Monitoring for providing help with field survey data.

Data Availability Statement: Data will be made available on request.

Conflicts of Interest: The authors declare no conflicts of interest.

References

- Mitchard, E.T.A. The tropical forest carbon cycle and climate change. *Nature* **2018**, *559*, 527–534. [[CrossRef](#)] [[PubMed](#)]
- Qu, Q.; Xu, H.; Ai, Z.; Wang, M.; Wang, G.; Liu, G.; Geissen, V.; Ritsema, C.J.; Xue, S. Impacts of extreme weather events on terrestrial carbon and nitrogen cycling: A global meta-analysis. *Environ. Pollut.* **2023**, *319*, 120996. [[CrossRef](#)] [[PubMed](#)]
- Zhao, Z.; Wang, X.; Li, R.; Luo, W.; Wu, C. Impacts of climate extremes on autumn phenology in contrasting temperate and alpine grasslands in China. *Agric. For. Meteorol.* **2023**, *336*, 109495. [[CrossRef](#)]
- Deng, Y.; Wang, X.; Lu, T.; Du, H.; Ciais, P.; Lin, X. Divergent seasonal responses of carbon fluxes to extreme droughts over China. *Agric. For. Meteorol.* **2023**, *328*, 109253. [[CrossRef](#)]
- Piao, S.; Wang, X.; Park, T.; Chen, C.; Lian, X.; He, Y.; Bjerke, J.W.; Chen, A.; Ciais, P.; Tømmervik, H.; et al. Characteristics, drivers and feedbacks of global greening. *Nat. Rev. Earth Environ.* **2020**, *1*, 14–27. [[CrossRef](#)]
- Yu, L.; Xue, Y.; Diallo, I. Vegetation greening in China and its effect on summer regional climate. *Sci. Bull.* **2020**, *66*, 13–17. [[CrossRef](#)]
- Bolla, B.; Manninger, M.; Molnár, T.; Horváth, B.; Szolgay, J.; Gribovszki, Z.; Kalicz, P.; Szabó, A. Evaluation of the compound effects of the 2022 drought and heatwave on selected forest monitoring sites in Hungary in relation to its multi-year drought legacy. *Forests* **2024**, *15*, 941. [[CrossRef](#)]
- Li, Z.; Xia, J.; Deng, X.; Yan, H. Multilevel modelling of impacts of human and natural factors on ecosystem services change in an oasis, Northwest China. *Resour. Conserv. Recycl.* **2021**, *169*, 105474. [[CrossRef](#)]
- Gong, W.; Huang, C.; Houghton, R.A.; Nassikas, A.; Zhao, F.; Tao, X.; Lu, J.; Schleeuwis, K. Carbon fluxes from contemporary forest disturbances in North Carolina evaluated using a grid-based carbon accounting model and fine resolution remote sensing products. *Sci. Remote Sens.* **2022**, *5*, 100042. [[CrossRef](#)]
- Pan, Y.; Birdsey, R.A.; Phillips, O.L.; Houghton, R.A.; Fang, J.; Kauppi, P.E.; Keith, H.; Kurz, W.A.; Ito, A.; Lewis, S.L.; et al. The enduring world forest carbon sink. *Nature* **2024**, *631*, 563–569. [[CrossRef](#)]
- Zhao, D.; Zhang, Z.; Zhang, Y. Soil moisture dominates the forest productivity decline during the 2022 China compound drought-heatwave event. *Geophys. Res. Lett.* **2023**, *50*, e2023GL104539. [[CrossRef](#)]
- Li, T.; Wang, S.; Chen, B.; Wang, Y.; Chen, S.; Chen, J.; Xiao, Y.; Xia, Y.; Zhao, Z.; Chen, X.; et al. Widespread reduction in gross primary productivity caused by the compound heat and drought in Yangtze River Basin in 2022. *Environ. Res. Lett.* **2024**, *19*, 034048. [[CrossRef](#)]
- Han, H.; Jian, H.; Liu, M.; Lei, S.; Yao, S.; Yan, F. Impacts of drought and heat events on vegetative growth in a typical humid zone of the middle and lower reaches of the Yangtze River, China. *J. Hydrol.* **2023**, *620*, 129452. [[CrossRef](#)]
- Pei, F.; Li, X.; Liu, X.; Lao, C. Assessing the impacts of droughts on net primary productivity in China. *J. Environ. Manag.* **2013**, *114*, 362–371. [[CrossRef](#)] [[PubMed](#)]
- Tian, R.; Li, J.; Zheng, J.; Liu, L.; Han, W.; Liu, Y. The impact of compound drought and heatwave events from 1982 to 2022 on the phenology of Central Asian grasslands. *J. Environ. Manag.* **2024**, *365*, 121624. [[CrossRef](#)]
- Zhu, L.; Meng, J.; Zhu, L. Applying Geodetector to disentangle the contributions of natural and anthropogenic factors to NDVI variations in the middle reaches of the Heihe River Basin. *Ecol. Indic.* **2020**, *117*, 106545. [[CrossRef](#)]
- Wang, J.; Xu, C. Geodetector: Principle and perspective. *Acta Geogr. Sin.* **2017**, *72*, 116–134. [[CrossRef](#)]

18. Xiao, J.; Chevallier, F.; Gomez, C.; Guanter, L.; Hicke, J.A.; Huete, A.R.; Ichii, K.; Ni, W.; Pang, Y.; Rahman, A.F.; et al. Remote sensing of the terrestrial carbon cycle: A review of advances over 50 years. *Remote Sens. Environ.* **2019**, *233*, 111383. [[CrossRef](#)]
19. Kang, J.; Zhang, B.; Dang, A. A novel geospatial machine learning approach to quantify non-linear effects of land use/land cover change (LULCC) on carbon dynamics. *Int. J. Appl. Earth Obs. Geoinf.* **2024**, *128*, 103712. [[CrossRef](#)]
20. Zeng, W.; Chen, X.; Yang, X. Estimating changes of forest carbon storage in China for 70 years (1949–2018). *Sci. Rep.* **2023**, *13*, 16864. [[CrossRef](#)]
21. Houghton, R.A.; House, J.I.; Pongratz, J.; van der Werf, G.R.; DeFries, R.S.; Hansen, M.C.; Le Quéré, C.; Ramankutty, N. Carbon emissions from land use and land-cover change. *Biogeosciences* **2012**, *9*, 5125–5142. [[CrossRef](#)]
22. Lu, H.; Wang, X.; Zhang, H.; Xie, X.; Nakhavali, M.; Quine, T.A.; Xu, W.; Xia, J.; He, B.; Hao, Z.; et al. Soil organic carbon lateral movement processes integrated into a terrestrial ecosystem model. *J. Adv. Model. Earth Syst.* **2024**, *16*, e2023MS003916. [[CrossRef](#)]
23. Zhao, B.; Zhuang, Q. Peatlands and their carbon dynamics in northern high latitudes from 1990 to 2300: A process-based biogeochemistry model analysis. *Biogeosciences* **2023**, *20*, 251–270. [[CrossRef](#)]
24. Houghton, R.; Hackler, J.; Lawrence, K. The U.S. carbon budget: Contributions from land-use change. *Science* **1999**, *285*, 574–578. [[CrossRef](#)]
25. Tang, X.; Hutyrá, L.R.; Arévalo, P.; Baccini, A.; Woodcock, C.E.; Olofsson, P. Spatiotemporal tracking of carbon emissions and uptake using time series analysis of Landsat data: A spatially explicit carbon bookkeeping model. *Sci. Total Environ.* **2020**, *720*, 137409. [[CrossRef](#)]
26. Gasser, T.; Crepin, L.; Quilcaille, Y.; Houghton, R.; Ciais, P.; Obersteiner, M. Historical CO₂ emissions from land use and land cover change and their uncertainty. *Biogeosciences* **2020**, *17*, 4075–4101. [[CrossRef](#)]
27. Hartung, K.; Bastos, A.; Chini, L.; Ganzenmüller, R.; Havermann, F.; Hurtt, G.C.; Loughran, T.; Nabel, J.E.M.S.; Nützel, T.; Obermeier, W.A.; et al. Bookkeeping estimates of the net land-use change flux—A sensitivity study with the CMIP6 land-use dataset. *Earth Syst. Dyn.* **2021**, *12*, 763–782. [[CrossRef](#)]
28. Yan, Y.; Wu, C.; Wen, Y. Determining the impacts of climate change and urban expansion on net primary productivity using the spatio-temporal fusion of remote sensing data. *Ecol. Indic.* **2021**, *127*, 107737. [[CrossRef](#)]
29. Feng, H.; Kang, P.; Deng, Z.; Zhao, W.; Hua, M.; Zhu, X.; Wang, Z. The impact of climate change and human activities to vegetation carbon sequestration variation in Sichuan and Chongqing. *Environ. Res.* **2023**, *238*, 117138. [[CrossRef](#)]
30. Wang, J.; Yan, R.; Wu, G.; Liu, Y.; Wang, M.; Zeng, N.; Jiang, F.; Wang, H.; He, W.; Wu, M.; et al. Unprecedented decline in photosynthesis caused by summer 2022 record-breaking compound drought-heatwave over Yangtze River Basin. *Sci. Bull.* **2023**, *68*, 2160–2163. [[CrossRef](#)]
31. Chang, X.; Xing, Y.; Wang, J.; Yang, H.; Gong, W. Effects of land use and cover change (LUCC) on terrestrial carbon stocks in China between 2000 and 2018. *Resour. Conserv. Recycl.* **2022**, *182*, 106333. [[CrossRef](#)]
32. Zhao, C.; Chen, S.; Jia, K.; Li, D.; Qin, B.; Sun, Y.; Zhang, H. Quantitative assessment of the impacts of climate change and human activity on the net primary productivity of subtropical vegetation: The case of Shaoguan, Guangdong, China. *Forests* **2023**, *14*, 2447. [[CrossRef](#)]
33. Liu, G.; Zhang, L.; He, B.; Jin, X.; Zhang, Q.; Razafindrabe, B.; You, H. Temporal changes in extreme high temperature, heat waves and relevant disasters in Nanjing metropolitan region, China. *Nat. Hazards* **2015**, *76*, 1415–1430. [[CrossRef](#)]
34. Chen, Y.; Cao, R.; Chen, J.; Liu, L.; Matsushita, B. A practical approach to reconstruct high-quality Landsat NDVI time-series data by gap filling and the Savitzky–Golay filter. *ISPRS-J. Photogramm. Remote Sens.* **2021**, *180*, 174–190. [[CrossRef](#)]
35. Cao, R.; Xu, Z.; Chen, Y.; Chen, J.; Shen, M. Reconstructing high-spatiotemporal-resolution (30 m and 8-Days) NDVI time-series data for the Qinghai–Tibetan Plateau from 2000–2020. *Remote Sens.* **2022**, *14*, 3648. [[CrossRef](#)]
36. Peng, S.; Ding, Y.; Wen, Z.; Chen, Y.; Cao, Y.; Ren, J. Spatiotemporal change and trend analysis of potential evapotranspiration over the Loess Plateau of China during 2011–2100. *Agric. For. Meteorol.* **2017**, *233*, 183–194. [[CrossRef](#)]
37. Peng, S.; Gang, C.; Cao, Y.; Chen, Y. Assessment of climate change trends over the Loess Plateau in China from 1901 to 2100. *Int. J. Climatol.* **2018**, *38*, 2250–2264. [[CrossRef](#)]
38. Tang, W.; He, J.; Qi, J.; Yang, K. A dense station-based, long-term and high-accuracy dataset of daily surface solar radiation in China. *Earth Syst. Sci. Data* **2023**, *15*, 4537–4551. [[CrossRef](#)]
39. Yang, J.; Huang, X. The 30 m annual land cover and its dynamics in China from 1990 to 2019. *Earth Syst. Sci. Data* **2021**, *13*, 3907–3925. [[CrossRef](#)]
40. Lai, L.; Huang, X.; Yang, H.; Chuai, X.; Zhang, M.; Zhong, T.; Chen, Z.; Chen, Y.; Wang, X.; Thompson, J.R. Carbon emissions from land-use change and management in China between 1990 and 2010. *Sci. Adv.* **2016**, *2*, e1601063. [[CrossRef](#)]
41. Yan, X.; Cai, Z. Number of soil profiles needed to give a reliable overall estimate of soil organic carbon storage using profile carbon density data. *Soil Sci. Plant Nutr.* **2008**, *54*, 819–825. [[CrossRef](#)]
42. Yang, J.; Xie, B.; Zhang, D. Spatio-temporal evolution of carbon stocks in the Yellow River Basin based on INVEST and CA-Markov models. *Chin. J. Eco-Agric.* **2021**, *29*, 1018–1029. [[CrossRef](#)]
43. Zhu, W.Q.; Pan, Y.; Zhang, J.S. Estimation of net primary productivity of Chinese terrestrial vegetation based on remote sensing. *J. Plant Ecol.* **2007**, *31*, 413–424. [[CrossRef](#)]
44. Wu, Y.; Yang, J.; Li, S.; Yu, H.; Luo, G.; Yang, X.; Yue, F.; Guo, C.; Zhang, Y.; Gu, L.; et al. The impact of climate change and human activities on the spatial and temporal variations of vegetation NPP in the hilly-plain region of Shandong Province, China. *Forests* **2024**, *15*, 898. [[CrossRef](#)]

45. Wang, Z.; Zhou, Y.; Sun, X.; Xu, Y. Estimation of NPP in Huangshan district based on deep learning and CASA model. *Forests* **2024**, *15*, 1467. [[CrossRef](#)]
46. Kindermann, G.; McCallum, I.; Fritz, S.; Obersteiner, M. A global forest growing stock, biomass and carbon map based on FAO statistics. *Silva Fenn.* **2008**, *42*, 244. [[CrossRef](#)]
47. Poepflau, C. Estimating root: Shoot ratio and soil carbon inputs in temperate grasslands with the rothc model. *Plant Soil* **2016**, *407*, 293–305. [[CrossRef](#)]
48. Cao, M.; Woodward, F.I. Dynamic responses of terrestrial ecosystem carbon cycling to global climate change. *Nature* **1998**, *393*, 249–252. [[CrossRef](#)]
49. Zhang, X.B.; Shangguan, Z.P. The bio-cycle patterns of nutrient elements and stand biomass in forest communities in hilly loess regions. *Acta Ecol. Sin.* **2005**, *25*, 527–537. [[CrossRef](#)]
50. Zhang, N.; Liang, Y.M. Studies on the below-ground/above-ground biomass ratio of natural grassland in loess hilly region. *Pratac. Sci.* **2002**, *11*, 72–78. [[CrossRef](#)]
51. Lu, N.; Akujärvi, A.; Wu, X.; Liski, J.; Wen, Z.; Holmberg, M.; Feng, X.; Zeng, Y.; Fu, B. Changes in soil carbon stock predicted by a process-based soil carbon model (Yasso07) in the Yanhe watershed of the Loess Plateau. *Landsc. Ecol.* **2015**, *30*, 399–413. [[CrossRef](#)]
52. Cai, A.; Chang, N.; Zhang, W.; Liang, G.; Zhang, X.; Hou, E.; Jiang, L.; Chen, X.; Xu, M.; Luo, Y. The spatial patterns of litter turnover time in Chinese terrestrial ecosystems. *Eur. J. Soil Sci.* **2020**, *71*, 856–867. [[CrossRef](#)]
53. Houghton, R.A.; Nassikas, A.A. Global and regional fluxes of carbon from land use and land cover change 1850–2015. *Glob. Biogeochem. Cycle* **2017**, *31*, 456–472. [[CrossRef](#)]
54. Yang, X.; Jin, X.; Xiang, X.; Fan, Y.; Liu, J.; Shan, W.; Zhou, Y. Carbon emissions induced by farmland expansion in China during the past 300 years. *Sci. China Earth Sci.* **2019**, *62*, 423–437. [[CrossRef](#)]
55. Zscheischler, J.; Orth, R.; Seneviratne, S.I. Bivariate return periods of temperature and precipitation explain a large fraction of European crop yields. *Biogeosciences* **2017**, *14*, 3309–3320. [[CrossRef](#)]
56. Guttman, N.B. Comparing the palmer drought index and the standardized precipitation index. *J. Am. Water Resour. Assoc.* **1998**, *34*, 113–121. [[CrossRef](#)]
57. Hao, Y.; Hao, Z.; Feng, S.; Zhang, X.; Hao, F. Response of vegetation to El Niño-Southern Oscillation (ENSO) via compound dry and hot events in southern Africa. *Glob. Planet. Change* **2020**, *195*, 103358. [[CrossRef](#)]
58. Han, D.; Wang, G.; Liu, T.; Xue, B.-L.; Kuczera, G.; Xu, X. Hydroclimatic response of evapotranspiration partitioning to prolonged droughts in semiarid grassland. *J. Hydrol.* **2018**, *563*, 766–777. [[CrossRef](#)]
59. Li, J.; Wang, Y.; Liu, L. Responses of the terrestrial ecosystem productivity to droughts in China. *Front. Earth Sci.* **2020**, *8*, 89. [[CrossRef](#)]
60. Tang, J.; Niu, B.; Hu, Z.; Zhang, X. Increasing susceptibility and shortening response time of vegetation productivity to drought from 2001 to 2021. *Agric. For. Meteorol.* **2024**, *352*, 110025. [[CrossRef](#)]
61. Ge, W.; Deng, L.; Wang, F.; Han, J. Quantifying the contributions of human activities and climate change to vegetation net primary productivity dynamics in China from 2001 to 2016. *Sci. Total Environ.* **2021**, *773*, 145648. [[CrossRef](#)] [[PubMed](#)]
62. Cai, Y.; Li, K. Spatiotemporal dynamic evolution and influencing factors of land use carbon emissions: Evidence from Jiangsu Province, China. *Front. Environ. Sci.* **2024**, *12*, 1368205. [[CrossRef](#)]
63. Chuai, X.; Yuan, Y.; Zhang, X.; Guo, X.; Zhang, X.; Xie, F.; Zhao, R.; Li, J. Multiangle land use-linked carbon balance examination in Nanjing City, China. *Land Use Policy* **2019**, *84*, 305–315. [[CrossRef](#)]
64. Zhao, R.; Huang, X.; Liu, Y.; Zhong, T.; Ding, M.; Chuai, X. Carbon emission of regional land use and its decomposition analysis: Case study of Nanjing City, China. *Chin. Geogr. Sci.* **2015**, *25*, 198–212. [[CrossRef](#)]
65. *China Forestry Statistical Yearbook*; China Forestry Publishing House: Beijing, China; Available online: <https://cnki.nbsti.net/CSYDMirror/trade/Yearbook/Single/N2006050899?z=Z010> (accessed on 14 March 2024).
66. Chen, J.; Gao, J.; Chen, W. Urban land expansion and the transitional mechanisms in Nanjing, China. *Habitat Int.* **2016**, *53*, 274–283. [[CrossRef](#)]
67. Sylvester, J.M.; Gutiérrez-Zapata, D.M.; Pérez-Marulanda, L.; Vanegas-Cubillos, M.; Bruun, T.B.; Mertz, O.; Castro-Nunez, A. Analysis of food system drivers of deforestation highlights foreign direct investments and urbanization as threats to tropical forests. *Sci. Rep.* **2024**, *14*, 15179. [[CrossRef](#)]
68. Mgelwa, A.S.; Ngaba, M.J.Y.; Hu, B.; Gurmesa, G.A.; Mwakaje, A.G.; Nyemeck, M.P.B.; Zhu, F.; Qiu, Q.; Song, L.; Wang, Y.; et al. Meta-analysis of 21st century studies shows that deforestation induces profound changes in soil characteristics, particularly soil organic carbon accumulation. *For. Ecosyst.* **2025**, *12*, 100257. [[CrossRef](#)]
69. Artaxo, P. Amazon deforestation implications in local/regional climate change. *Proc. Natl. Acad. Sci. USA* **2023**, *120*, e2317456120. [[CrossRef](#)]
70. Xu, H.; Yue, C.; Piao, S. Future forestation in China should aim to align the temporal service window of the forest carbon sink with the “carbon neutrality” strategy. *Sci. China Earth Sci.* **2023**, *66*, 2971–2976. [[CrossRef](#)]
71. Wang, D.; Alimohammadi, N. Responses of annual runoff, evaporation, and storage change to climate variability at the watershed scale. *Water Resour. Res.* **2012**, *48*, W05546. [[CrossRef](#)]
72. Wang, H.; Yan, S.; Liang, Z.; Jiao, K.; Li, D.; Wei, F.; Li, S. Strength of association between vegetation greenness and its drivers across China between 1982 and 2015: Regional differences and temporal variations. *Ecol. Indic.* **2021**, *128*, 107831. [[CrossRef](#)]

73. Zscheischler, J.; Mahecha, M.D.; von Buttlar, J.; Harmeling, S.; Jung, M.; Rammig, A.; Randerson, J.T.; Schölkopf, B.; Seneviratne, S.I.; Tomelleri, E.; et al. A few extreme events dominate global interannual variability in gross primary production. *Environ. Res. Lett.* **2014**, *9*, 035001. [[CrossRef](#)]
74. Sharma, S.; Mujumdar, P. Increasing frequency and spatial extent of concurrent meteorological droughts and heatwaves in India. *Sci. Rep.* **2017**, *7*, 15582. [[CrossRef](#)] [[PubMed](#)]
75. Matkala, L.; Kulmala, L.; Kolari, P.; Aurela, M.; Bäck, J. Resilience of subarctic Scots pine and Norway spruce forests to extreme weather events. *Agric. For. Meteorol.* **2021**, *296*, 108239. [[CrossRef](#)]
76. Xiao, L.; Wu, X.; Zhao, S.; Zhou, J. Memory effects of vegetation after extreme weather events under various geological conditions in a typical karst watershed in southwestern China. *Agric. For. Meteorol.* **2024**, *345*, 109840. [[CrossRef](#)]
77. Roy, P.; Pal, S.C.; Chakraborty, R.; Chowdhuri, I.; Saha, A.; Shit, M. Climate change and groundwater overdraft impacts on agricultural drought in India: Vulnerability assessment, food security measures and policy recommendation. *Sci. Total Environ.* **2022**, *849*, 157850. [[CrossRef](#)]
78. Gazol, A.; Camarero, J.J. Compound climate events increase tree drought mortality across European forests. *Sci. Total Environ.* **2022**, *816*, 151604. [[CrossRef](#)]
79. Delphin, S.; Escobedo, F.J.; Abd-Elrahman, A.; Cropper, W.P. Urbanization as a land use change driver of forest ecosystem services. *Land Use Policy* **2016**, *54*, 188–199. [[CrossRef](#)]
80. Xu, Q.; Yang, R.; Dong, Y.-X.; Liu, Y.-X.; Qiu, L.-R. The influence of rapid urbanization and land use changes on terrestrial carbon sources/sinks in Guangzhou, China. *Ecol. Indic.* **2016**, *70*, 304–316. [[CrossRef](#)]
81. Zhang, M.; Tan, S.; Liang, J.; Zhang, C.; Chen, E. Predicting the impacts of urban development on urban thermal environment using machine learning algorithms in Nanjing, China. *J. Environ. Manag.* **2024**, *356*, 120560. [[CrossRef](#)]
82. Wang, L.-J.; Luo, G.-Y.; Ma, S.; Wang, H.-Y.; Jiang, J.; Zhang, J.-G. Integrating landscape ecological risk into ecosystem service value assessment: A case study of Nanjing City, China. *Ecol. Indic.* **2023**, *154*, 110625. [[CrossRef](#)]
83. Chuai, X.; Huang, X.; Lu, Q.; Zhang, M.; Zhao, R.; Lu, J. Spatiotemporal changes of built-up land expansion and carbon emissions caused by the Chinese construction industry. *Environ. Sci. Technol.* **2015**, *49*, 13021–13030. [[CrossRef](#)] [[PubMed](#)]
84. Li, J.; Guo, X.; Chuai, X.; Xie, F.; Yang, F.; Gao, R.; Ji, X. Reexamine China's terrestrial ecosystem carbon balance under land use-type and climate change. *Land Use Policy* **2021**, *102*, 105275. [[CrossRef](#)]
85. Xiong, K.; Chi, Y. The problems in southern China karst ecosystem in southern of China and its countermeasures. *Ecol. Econ.* **2015**, *31*, 23–30.
86. Li, S.-L.; Liu, C.-Q.; Chen, J.-A.; Wang, S.-J. Karst ecosystem and environment: Characteristics, evolution processes, and sustainable development. *Agric. Ecosyst. Environ.* **2021**, *306*, 107173. [[CrossRef](#)]
87. Wang, J.; Liang, P.; Cheng, F.; Liu, Y.; Song, C.; Wu, W.; Zheng, Q.; Zhang, T.; Qu, P.; Li, Y.; et al. Evaluation and projection of circulation conditions tied to summertime compound drought and heatwave frequency over the Yangtze River Delta, China, for the carbon neutrality period based on CMIP6 GCMs. *Int. J. Climatol.* **2024**, *44*, 2739–2757. [[CrossRef](#)]
88. Winckler, J.; Reick, C.H.; Luyssaert, S.; Cescatti, A.; Stoy, P.C.; Lejeune, Q.; Raddatz, T.; Chlond, A.; Heidkamp, M.; Pongratz, J. Different response of surface temperature and air temperature to deforestation in climate models. *Earth Syst. Dyn.* **2019**, *10*, 473–484. [[CrossRef](#)]
89. Mukherjee, S.; Mishra, A.K. Increase in compound drought and heatwaves in a warming world. *Geophys. Res. Lett.* **2021**, *48*, e2020GL090617. [[CrossRef](#)]
90. Zhang, Z.; Wang, X.; Zhang, Y.; Gao, Y.; Liu, Y.; Sun, X.; Zhi, J.; Yin, S. Simulating land use change for sustainable land management in rapid urbanization regions: A case study of the Yangtze River Delta region. *Landsc. Ecol.* **2023**, *38*, 1807–1830. [[CrossRef](#)]
91. Liu, C.; Hu, S.; Wu, S.; Song, J.; Li, H. County-level land use carbon emissions in China: Spatiotemporal patterns and impact factors. *Sust. Cities Soc.* **2024**, *105*, 105304. [[CrossRef](#)]
92. Davis, K.F.; Koo, H.I.; Dell'Angelo, J.; D'Odorico, P.; Estes, L.; Kehoe, L.J.; Kharratzadeh, M.; Kuemmerle, T.; Machava, D.; Pais, R.; et al. Tropical forest loss enhanced by large-scale land acquisitions. *Nat. Geosci.* **2020**, *13*, 482–488. [[CrossRef](#)]
93. Ameray, A.; Bergeron, Y.; Valeria, O.; Montoro Girona, M.; Cavard, X. Forest Carbon Management: A review of silvicultural practices and management strategies across boreal, temperate and tropical forests. *Curr. For. Rep.* **2021**, *7*, 245–266. [[CrossRef](#)]
94. Wu, C.; Chen, K.; E, C.; You, X.; He, D.; Hu, L.; Liu, B.; Wang, R.; Shi, Y.; Li, C.; et al. Improved CASA model based on satellite remote sensing data: Simulating net primary productivity of Qinghai Lake basin alpine grassland. *Geosci. Model Dev.* **2022**, *15*, 6919–6933. [[CrossRef](#)]
95. Chen, T.; Wang, Y.; Peng, L. Advanced time-lagged effects of drought on global vegetation growth and its social risk in the 21st century. *J. Environ. Manag.* **2023**, *347*, 119253. [[CrossRef](#)] [[PubMed](#)]

Disclaimer/Publisher's Note: The statements, opinions and data contained in all publications are solely those of the individual author(s) and contributor(s) and not of MDPI and/or the editor(s). MDPI and/or the editor(s) disclaim responsibility for any injury to people or property resulting from any ideas, methods, instructions or products referred to in the content.